Frontiers in Scientific Research and Technology

Online ISSN: 2682-2970
Print ISSN: 2682-2962
http://fsrt.journals.ekb.eg

FSRT J 9 (2024) 14 - 24 10.21608/FSRT.2024.278732.1122

Synthesis and evaluation of linseed and coconut oil derivatives as protective coating for outdoor iron-based artifacts

Wafaa A. Mohamed[1], Gehad M. Mohamed[2,*]

[1] Conservation Department, Faculty of Archaeology, Cairo University, 12613, Giza, Egypt

[2] Ministry of Antiquities, Zamalek, Cairo, Egypt.

ARTICLE INFO

Article history:
Received 22 March 2024
Received in revised form 13 April 2024
Accepted 20 April 2024
Available online 28 April 2024

Keywords
Vegetable oil derivatives;
eco-friendly coating;
outdoor iron artefacts;
lamp post;
low carbon steel (LCS).

ABSTRACT

Many strategies for efficient, eco-friendly, reversible, and protective coating preparation were proposed in the last decades for the protection of outdoor archaeological metal artifacts. Herein, vegetable oil derivatives (VO) were easily synthesized through one step by reaction of ozonation and amination of triglyceride (TGO) to prepare modified oil coatings (MOC). VO samples and chemical structure were confirmed using FT-IR and UV. The mitigation power of TGO, and MOC for historic wrought iron (low Carbone steel (LCS)) in 3.5% NaCl solution was evaluated by artificial coupon, This coupon was prepared according to the chemical composition of a historical iron-based lamp post located at the Al-Shennawy Palace in Mansoura city, Dakahlia Governorate, Egypt, as an applied example for archaeological study." Electrochemical Impedance Spectroscopy (EIS) and dynamic Polarization (PDP) techniques were employed for this evaluation. The coated film underwent several tests, including a salt spray test, adhesion test, and aging test, based on ASTM standards. The protective capacity of the linseed oil of MOC increased to 75.6%, reflecting the blocking of active metal sites through the coating process.

1. Introduction

The preservation of archaeological metal specially outdoor artifacts is a complex task that requires the use of appropriate protective coatings should typically follow the universal standards and guidance for conservation of archaeological materials which include: transparency, reversibility, compatibility with the surface, long-term protection, easy synthesis, low cost, and non-toxicity [1][2], while industrial coatings offer high resistance, good mechanical properties and long-lasting they may not be suitable for application in the field of archaeology, Using linseed oil and coconut oil refers to testing the modifications applied in this study on two different kinds of oil from chemical and physical properties, with linseed oil as an example of a drying oil and coconut oil as an example of a non-drying oil.

The distinct properties of flaxseed oil and coconut oil can influence the synthesis of rust-protective coatings [3]. The high content of polyunsaturated fats in flaxseed oil, particularly α-linolenic acid, contributes to its drying properties. This makes flaxseed oil suitable for creating coatings that can dry and harden, providing a protective layer against rust [4].

On the other hand, coconut oil, with its high saturated fat content, is non-drying.

This means it remains in a semi-solid state, which may not be ideal for creating hard, protective coatings. However, its oxidation resistance could potentially contribute to the longevity of the coating [5].

In the present study, VO (linseed and coconut) derivatives were easily produced in simple steps (condensation reaction) which displays a good solubility for corrosion protection as coatings for *LCS* in 3.5% NaCl solution. The mitigation effect of the synthesized VO (linseed and coconut) derivatives on *LCS* corrosion behavior in 3.5% NaCl solution was evaluated using EIS, and PDP techniques, besides several coating tests (MOC).

2. Experimental methods

2.1. Synthesis of coating

2.1.1. Synthesis of primitive-based oil (TGO)

Extraction of various fats was done by adding 20 gm of linseed oil, coconut oil, and 0.4 mol/L KOH-CH_3OH solution were added to a 500 ml round-bottom flask. Using a thermostatic magnetic stirrer, mix and reflux the solution for approximately one hour at 65°C until it becomes clear and transparent. After the solution was moved to a beaker to cool to room temperature, the upper oil phase was separated using a separatory funnel, as shown in Fig. 1, and $NaHSO_4$ solution was added dropwise to bring the pH down to 3 [6].

* Corresponding author at Ministry of Antiquities

E-mail addresses: Gehadmamdouh_con@outlook.com (Gehad M. Mohamed)

2.1.2. Synthesis of oil-based coating (MOC)

The primitive-based oils (Coconut, and linseed) are exposed to UV and O_3 through ozonation [7, 8] process for 24 hours to provide carboxylic terminals (COOH), followed by amination reaction using (ethylene diamine) [9,10], as shown in Fig. 2.

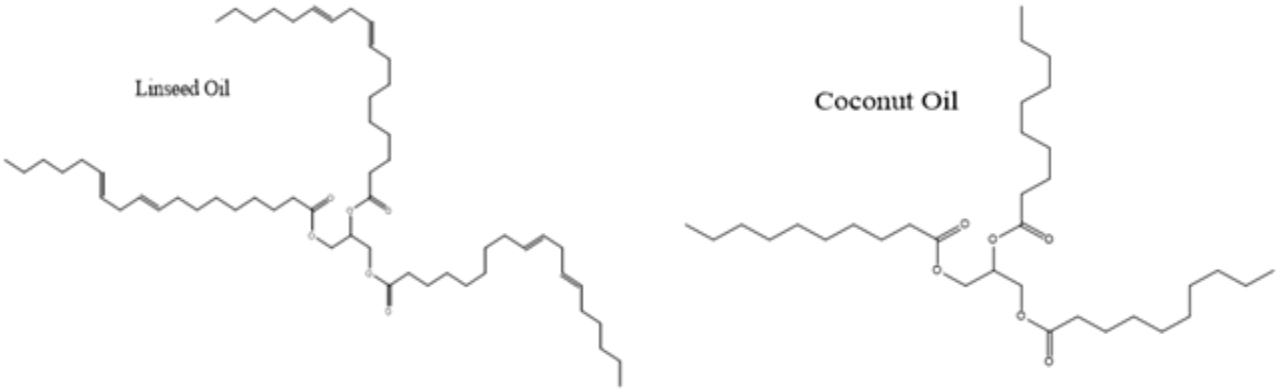

Fig.1. Oil Triglyceride (TGO)

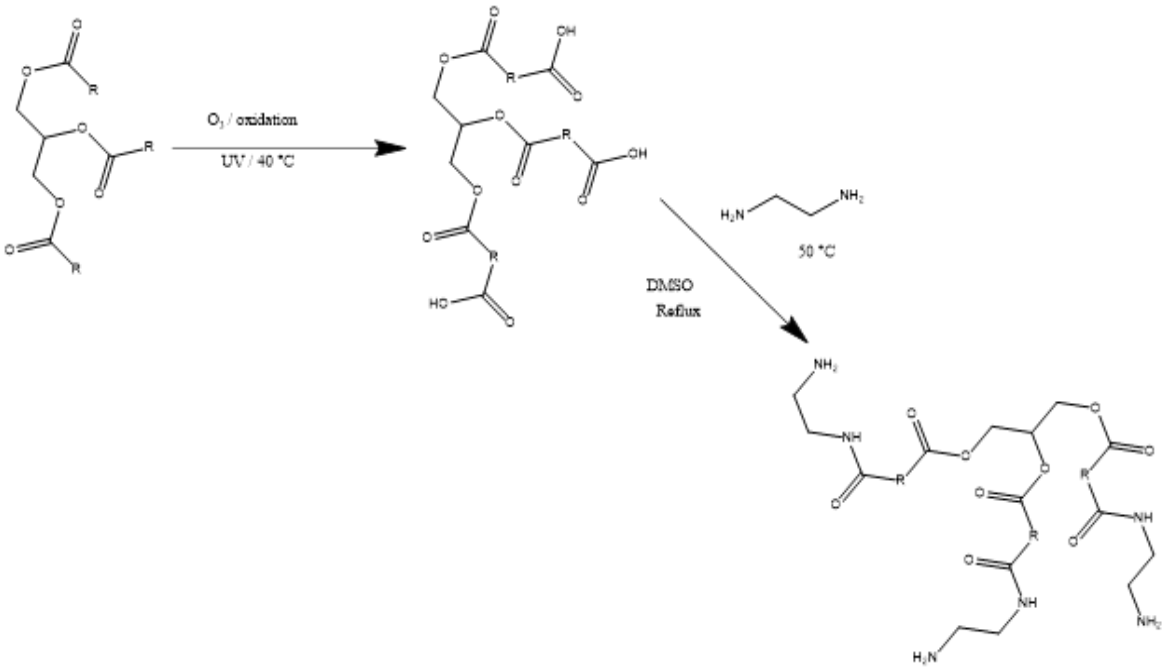

Fig.2. Oil based coating Synthesis (MOC)

2.1.3. Synthesis of modified oil-based coat

The prepared samples (~30%) are dissolved in a mixture solvent of DMF, hexane, and ethanol (~69.8%) with addition of UV resistant (benzophenone as photo-initiator) [11] and (triethanolamine as sealant agent) (~0.2%) with continuous stirring for 2 hours at 30 ^{O}C.

2.2. Coupon's composition and electrolytes.

LCS ingredients according to the historical lamp post alloy (wt%) are: (C: 0.03, Cr: 0.023, Si: 0.012, P: 0.042, Mn: 0.211, and Fe balanced) were determined by 2 methods. The 1st method is scanning the surface of the sample by scanning electron microscope (Model Quanta™ 3D 200i) to examine the morphology of the historical alloy before conservation and coating application, and analysis of the surface by energy dispersive x-ray diffraction (EDX) an attached unit with SEM microscope with software Thermofisher Pathfinde) to detect the elements concentrated on the alloy surface as seen in Fig. 3. The 2nd method is the atomic emission spectroscopy AES (Model SPECTRO MAXx) to determine the elemental analysis of the alloy accurately. Before every experiment, the LCS electrode is pretreated with varying grades of emery paper (400–2500) to create a mirror image. It is then cleaned with acetone and filtered water. The coating was applied by brush on the surface of the coupons at room temperature (40 ^{o}C ± 2 ^{o}C).

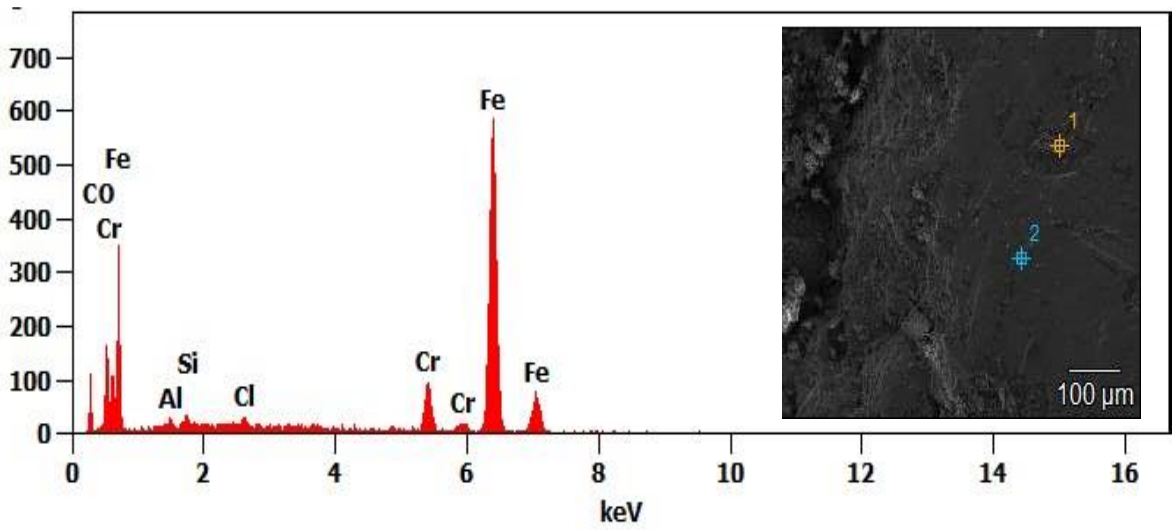

Fig. 3. SEM micrograph and EDX scan analysis of the case study alloy (historical lamp post)

2.3. Characterizations

The chemical structure of the coating samples was investigated through several techniques. Fourier Transform Infrared (FT-IR) was used for investigating the functional groups using Nicolet IS 400 using KBr as support from 4000-400 cm^{-1}. Ultraviolet/ visible spectroscopy (UV/Vis) was used to investigate the spectral absorbance using Shimadzu from 200-800 nm.

With the use of METROHM PGSTAT 1500, the electrochemical attitude of LCS in an aggressive solution 3.5% NaCl free and containing different coatings of VOs derivatives was investigated using EIS and Tafel techniques. Platinum wire was used as the axillary electrode, and Ag/AgCl was used as a reference electrode connected to LCS as the working electrode. The LCS electrochemical measurements were carried out in the presence and absence of various Vos coatings following the 30-minute OCP (open circuit potential) period. The EIS technique was used with an amplitude of 5 mV and a frequency range of 100 kHz: 0.01 Hz. A few of the corrosion reaction's kinetic characteristics, including charge transfer resistance (Rct) and solution resistance (Rs), were noted. The surface morphology of an LCS sample (1 x 1 x 0.3 cm) was examined using the SEM technique after 6 hours utilizing QUANTA FEG 250 to learn more about the LCS corrosion process and the protective ability of the produced coating.

2.3.1 Mechanical Characterizations

1. Coating Mechanical properties tested throw the adhesion strength of the synthesized coatings which were tested in the study using two methods. The first method involved measuring the adhesion strength of the coatings by pulling with a Posi Meter (Pull-off Adhesion Tester) Posi Test AT-A, Automatic adhesion tester model DeFelsko according to ASTM D4541 [12] standard, this method aims to monitor the mechanical properties of the coating by indicating the specific adhesion strength through the device, which depends on measuring the coating's resistance to pull force. The device monitors the coating's resistance to pull-off force, expressing it in N/mm.
2. The second method for determining the adhesion strength of the synthesized coatings using (cross-cut adhesion test) according to ASTM D3359[13] standard. This test expresses differently the adhesion strength of the coatings to the alloy surface and some morphological properties of the coating, such as surface coverage strength, which is affected by time factors realistically.
3. Salt spray test according to (ASTM B117) standard [14] was tested through ATLAS SF-260.
4. Aging test according to (ASTM-G154) standard [15] was tested through UV test chamber Model: YUV-080 thin Monitoring the color change of tested coating.

3. Results and discussion

3.1 Chemical Characterizations

FT-IR of TGO (linseed, coconut) is shown in Fig.4, where the coconut oil shows vibration bands that appeared at 2904-2951 cm^{-1}, which are related to -CH aliphatic stretching bands. An overtone at ~1758 cm^{-1}, and 1563 cm^{-1} are related to the C=C, C=O of the triglyceride component of oil. Bands at ~1134 cms^{-1} are related to aliphatic -CH bending, while C-O band appears at ~1080 cm^{-1} [17]. Linseed oil shows vibration bands appeared at 2920-2840 cm^{-1}, which are related to -CH aliphatic stretching bands. An overtone at ~1730 cm^{-1}, and 1460 cm^{-1} are related to the C=C, C=O of the triglyceride component of oil. Bands at ~1150 cm^{-1} are related to aliphatic -CH bending, while C-O band appears at ~1095 cm^{-1} [18]. The prepared MOC showed the same bands of oils besides the presence of –NH group at >3200 cm^{-1}, owing to the presence of primary and secondary amine groups at oil coatings.

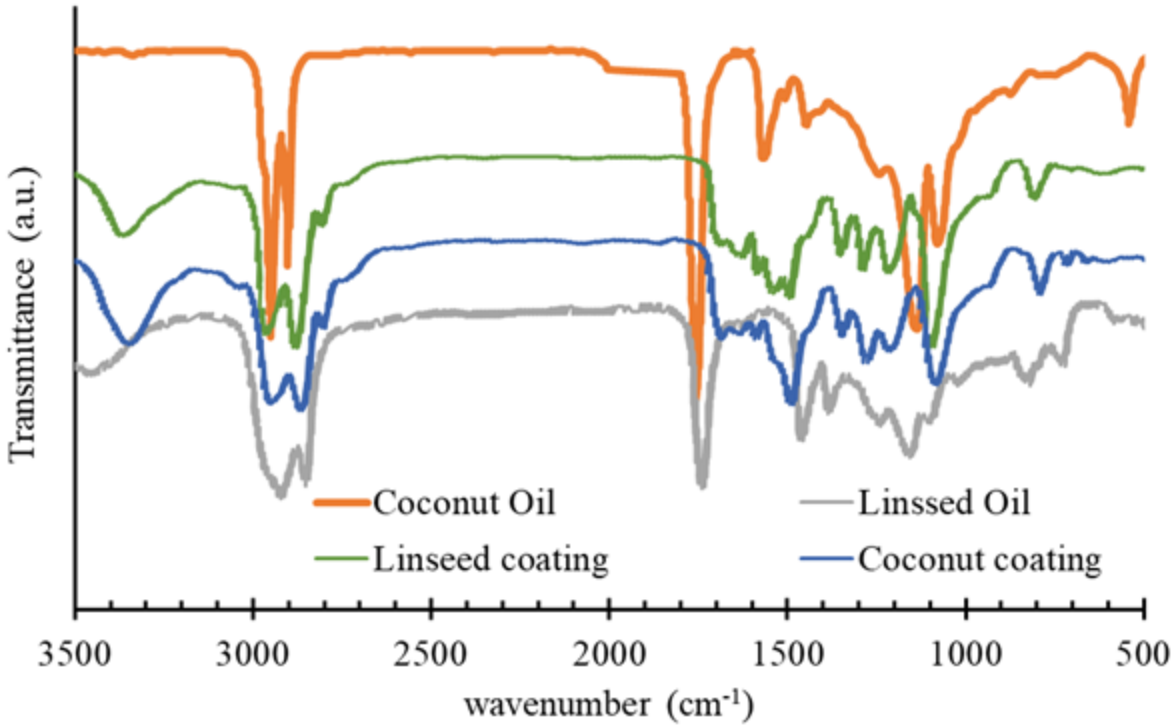

Fig.4. FT-IR of the prepared sample

The UV/vis spectra of samples were done in ethanol solution and plotted in Fig. 5. The absorption bands showed by the compounds. The electronic absorption spectrum of samples shows strong absorption bands with 2 maxima at 231.3 nm (coconut TGO), and 232.2 nm (linseed TGO), which are assigned to π→π* transition of the aliphatic C=C, and C=, besides band at 332 nm, which attributed to the n→π* transition between the lone pair of electrons of O and the carbonyl groups. The MCO samples show the same bands of TGO with some decrement of UV absorbance owing to the UV blocker additives added in the coating composition, besides making a shift for bands towards the visible light region and showing the band at 274 nm.

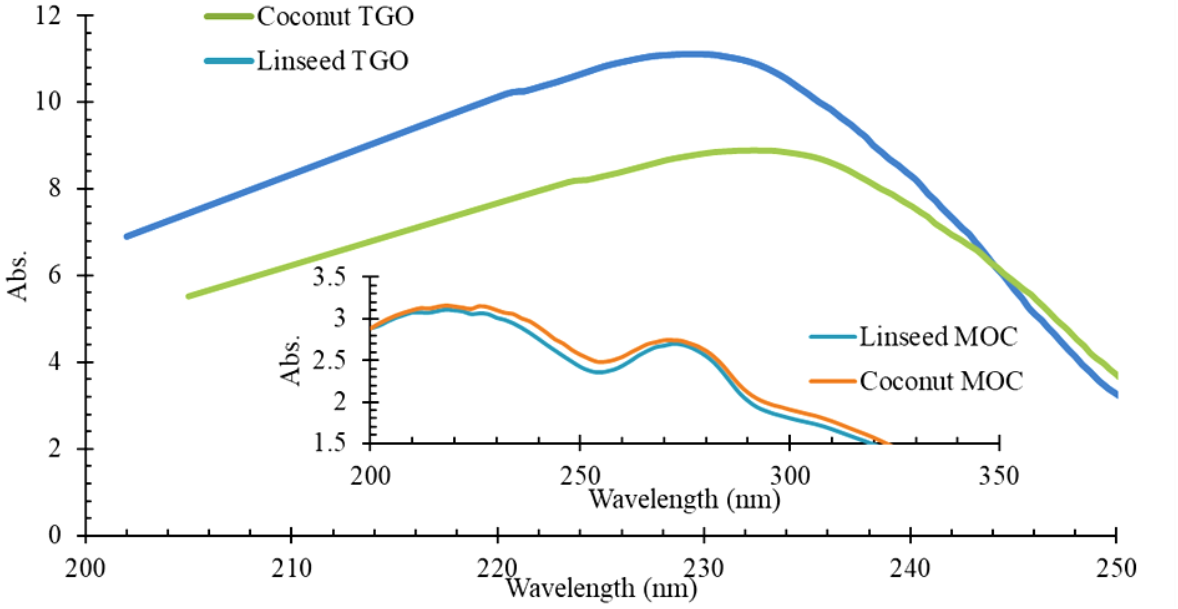

Fig. 5. UV/Vis of the prepared sample

3.1. Electrochemical measurements (EIS and PDP)

3.1.1. EIS analysis

Using a non-destructive EIS technique based on AC (alternative current), the corrosion process of the LCS (3.5% NaCl) contact was examined at room temperature (20 °C). The LCS Nyquist diagrams in 3.5% NaCl were displayed as shown in Figure 6. Semicircles with imperfections were Nyquist curves. These observations were linked to the frequency dispersion phenomenon, which is explained by the distribution of active sites, inhomogeneity, and roughness of the LCS [16]. A depressed capacitive semicircle is included in the LCS Nyquist curves in Figure 7. This suggests that Rct (charge transfer resistance) regulated the corrosion response mechanism of LCS and that coating variation altered it [17]. The variation in the diameter of Nyquist curves across different coatings can be attributed to an increase in LCS surface coverage, which in turn slows down the rate of LCS dissolution [18]. [19]. This behavior can be explained by the protective layer of TGO that forms over the LCS surface to shield it from the corrosive electrolyte. The molecules of MOC coatings then reduce direct contact between the aggressive media and the LCS surface through the adsorption process using their active centers, which include hetero atoms (nitrogen atoms) and π-electrons.

The coatings provide the CS surface with excellent protection. The values of θ (surface coverage) and η (corrosion protection efficiency) in Table 1 exhibit this behavior. Equations and Rct values were used to calculate the values of θ and η:

$$\theta = (Rct.inh - Rct.blank)/Rct.inh)$$

$$\eta = \theta \times 100$$

where the charge transfer resistances of the coatings and the blank solution are, respectively, $R_{ct.inh}$ and $_{Rct.blank}$. Table 1 illustrates how the addition of coatings increases the Rct value. This is explained by the fact that more coating molecules are adhering to the LCS surface and replacing corrosive molecules (H_2O and Cl^-).

3.1.2. Potentiodynamic Polarization (PDP)

As seen in Fig. 8, PDP was used to investigate the anti-corrosion behavior of coatings for LCS in aggressive 3.5% NaCl to learn more about the anodic and cathodic reactions. Coatings cause the anodic and cathodic Tafel lines to move in a noble direction, or to lower values. The high adsorption capacity of coatings to cover the LCS surface is responsible for this observation [20]. The difference between the coatings' I-V curves and the blank solutions, shows that the coatings' presence suppresses the LCS corrosion process [21]. By obstructing the active sites of LCS, coatings can mitigate the corrosion of LCS in a hostile environment, as shown by the parallel lines of the I-V curves in the cathodic area of Fig. 9. By sheltering the LCS surface with a coating layer, the blocking effect of coatings reduces the available surface area for Na^+, which in turn causes a drop in the rate of OH^- formation that cause the metal hydroxide followed by oxide formation. Therefore, the LCS response mechanism remains the same, and H_2 reduction is an activated control. The anodic Tafel lines in the anodic area provide information regarding the coatings inhibitor's ability to shield LCS from hostile environments. At the same time, the coatings inhibitor's ability to prevent corrosion at low anodic potential is dependent on the pace at which coatings are absorbed and form a protective layer. when the anodic potential is > -244 mV [22].

The electrochemical kinetic parameters derived from Tafel extrapolation of PDP curves are displayed in Table 1. Table 2's θ and η values were computed using the following equation about the I_{corr} value.:

$$\theta = (I\text{corr.blank} - I\text{corr.inh})/I\text{corr.blank}$$

$$\eta = \theta \times 100$$

The data presented in Table 2 illustrates the ability of coatings to mitigate LCS in a harsh NaCl solution. Coatings cause the I_{corr} value to go downward. This behavior indicates that well-adhered coatings on the LCS surface slow down the rate of corrosion by reducing the amount of time that corrosive particles encounter the surface and creating a protective layer. Following coatings, there was a modest impact on the anodic and cathodic Tafel slopes, but there was no significant change in the βa and βc values as shown in Table 1, suggesting that the LCS corrosion reaction mechanism remained unchanged. Furthermore, the shift in the E_{corr} value (less than 85 mV) indicates that VO functions as an anodic inhibitor for LCS in a 3.5% NaCl solution by obstructing the anodic sites on the surface of LCS [23].

Using SEM photomicrograph analysis, a potent tool that is complementary to electrochemical measurements (EMs), the surface analysis of the LCS was investigated. After immersion for six hours, the LCS was shown in two dimensions (Fig. 10), illustrating the destructive action of corrosive media (3.5% NaCl) and the mitigating role of coatings. Due to the media's destructive effect, SEM pictures showed the mitigation process of untreated LCS in 3.5% NaCl with severely damaged surfaces and corrosion products [24]. Using coatings, the anticorrosion behavior was verified. The LCS surface is visibly smoother and less prone to corrosion products (iron oxides and chlorides) than it was in the untreated solution (3.5% NaCl). This modification demonstrates how the LCS surface is shielded from corrosive particles by the creation of a protective film barrier, which reduces the amount of interaction between the LCS surface and media [25].

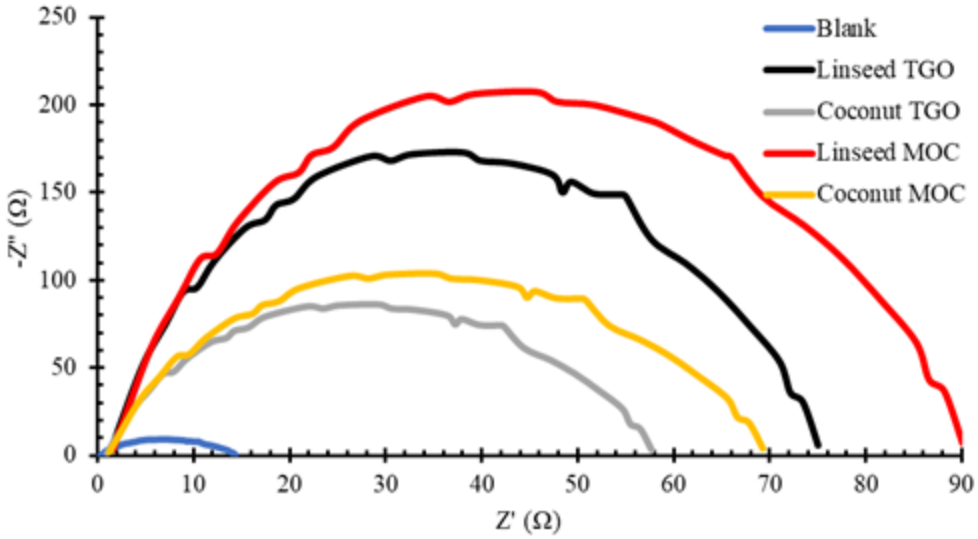

Fig.6. EIS of the tested coatings

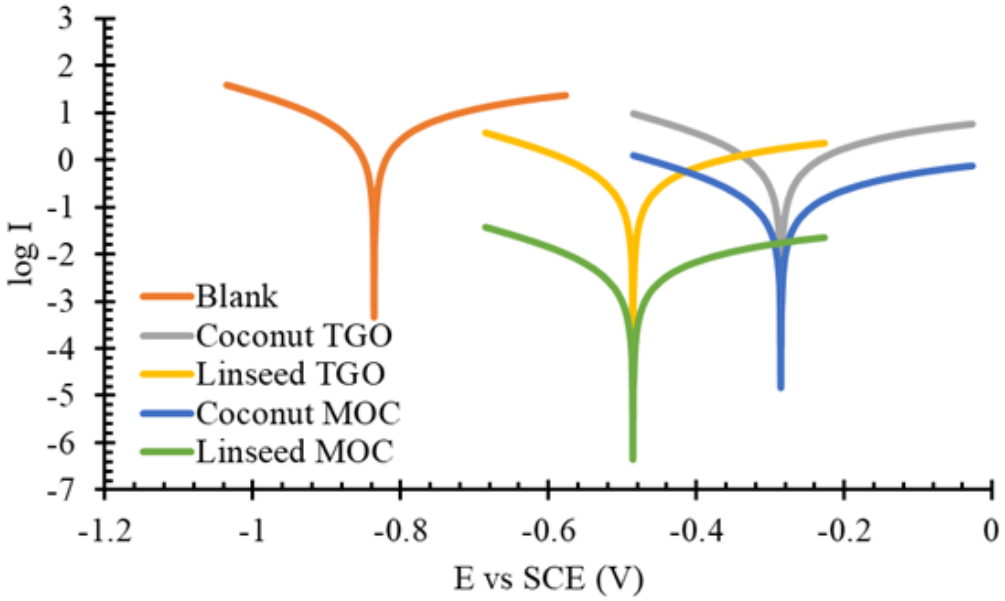

Fig. 7. Tafel analysis of the tested coatings

Table 1. Electrochemical measurements of the tested coatings

	PDP		EIS		
	- E_{corr} (V)	**IE (%)**	**R_s (Ω cm^2)**	**R_{ct} (Ω/cm^2)**	**IE (%)**
Blank	0.84	----	2	20.7	----
Linseed TGO	0.48	68.6	3.6	75	72.4
Coconut TGO	0.28	64.2	3.1	56.1	63.1
Linseed MOC	0.49	73.6	3.6	85	75.6
Coconut MOC	0.27	71.2	3.1	65	68.2

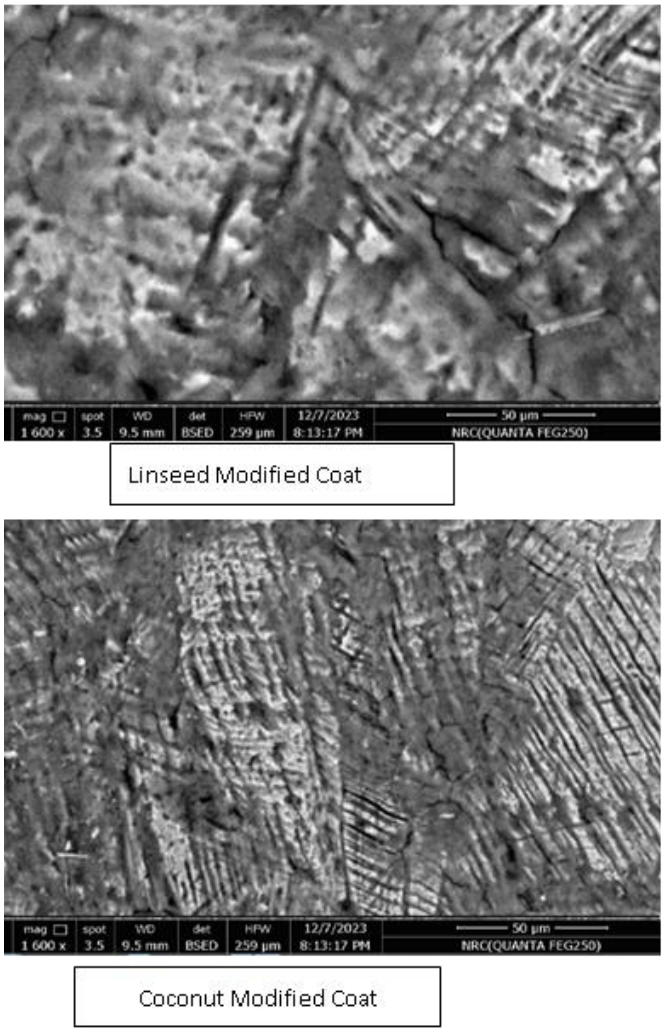

Fig. 8. SEM photomicrograph for MOC samples

3.3. Coating Mechanical characterization

3.3.1 Pull-off adhesion test

In adhesion testing, the main objective is to cause a coating failure. In a multi-layer application, the coating under test may encounter an interface failure between the coating and substrate or between the coating layers individually. A cohesive failure of coatings can also occur inside a specific layer. An adhesive is said to be perfect if it can form a stronger bond than the coating's failure point at both the adhesive-to-dolly and adhesive-to-coating interfaces. This guarantees the validity and significance of every pull test result.

Pre-testing the adhesive on the coating is also crucial to make sure it doesn't cause any discernible changes to the coating's characteristics. This test needs to be carried out as soon as the adhesive is completely mixed, applied to the coating, and allowed to cure. Any modification to the coatings' characteristics could render the findings void. As shown in Fig. 9, in one instance the adhesive seemed to react with the coating, strengthening its binding strength once the new compound completely hardened.

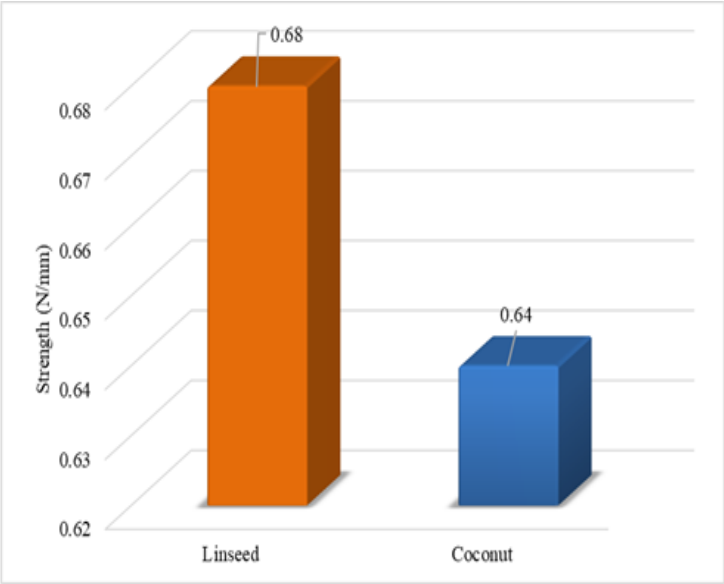

Fig. 9. Adhesion test for modified coatings (MOC)

3.3.2 Cross-cut adhesion test (tape test)

The measurements were carried out according to method B in (ASTM D3359). Adhesive (50 mm width × 50 mm length) is applied to the sample slices and then rolled horizontally back and forth three times to allow the adhesive lines to bond. This is done to study the adhesion strength of the coating on the surface of the samples under study. The results of the cracking test, after repeating the experiment 3 times, show that the coatings have stability from average to good. The results are presented in expresses the test results where the scale monitors the adhesion strength of each coating according to the adopted standard.

As seen in Fig.10, and Table 2 the prepared coating has high adhesion property as noticed. The thicker line refers to some adhesion problems but it's almost not noticeable. Some air bubbles are noticed that refer to some adhesion defects. The modified coating shows an unorganized line without any appearance of bubbles which refers to the good adhesive property, besides the good surface homogeneity of coatings.

3.3.3 Salt Spray test

The salt solution is prepared by dissolving 5 ± 1 parts weight of sodium chloride in 95 parts of water. The air supplied to the nozzle for spraying the salt solution should be free of oil and dirt and maintained between 69 and 172 kilonewtons/m^2 (10 and 25 pounds per square inch). The test result should be satisfactory if, after 30 minutes of drying when removed from the fog and spray, the paint does not show any peeling, and no more than 0.125 inches (3.2 mm) of paint can be removed in any direction from the area surrounding the scratch by pulling with a transparent plastic strip.

The performance of the paint is tested and evaluated over different periods, taking into account several factors including the intended use of the paint in addition to the relevant application standards. Fig.11. refer to the metal slides (uncoated) exposed to the salt spray test before and after exposure to test conditions.

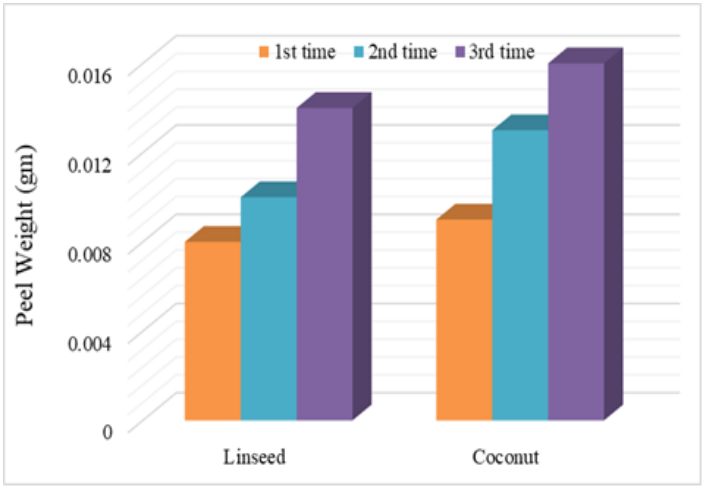

Fig.10. Cross-cut test for the tested coating (MOC)

Table 2. Cross- cut test result for modified coating (MOC

COATING (MOC)	PEELING (gm) ± 0.001gm			Classification of Adhesion degree of the coats
	1st time	2nd time	3rd time	
Linseed modified	0.008	0.01	0.014	4B
Coconut modified	0.016	0.013	0.64	4B

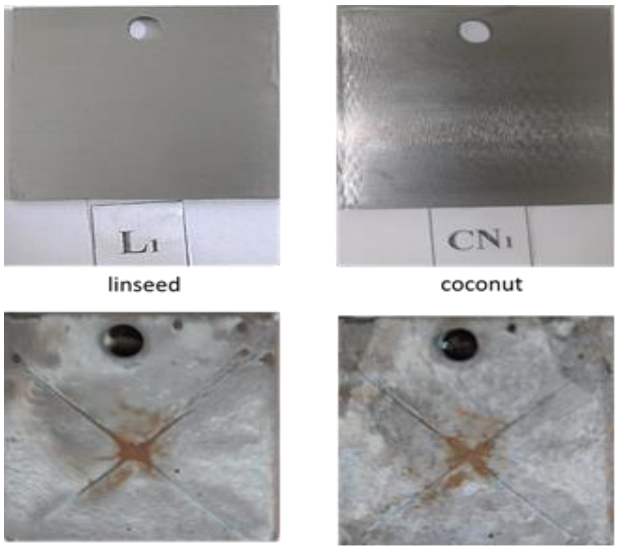

Fig. 11. Salt spray tests for the tested coatings before and after test

3.3.4 Accelerated aging test (UV test)

An accelerated UV aging test chamber is typically used in a laboratory to assess the resistance of new items to ultraviolet radiation using an ultraviolet aging test. Generally speaking, nonmetallic materials and organic materials (coatings, paints, dyes, fabrics, printing and packaging, adhesives, cosmetics, metals, electronics, electroplating, rubber, plastics, and other materials goods, etc.) are the products and materials that need to be tested for UV resistance.

Coating cracking, gloss loss, fading, yellowing, and chalking are primarily caused by prolonged exposure to outside sunshine, high temperatures, and high humidity. The spectral sensitivity of the coating's parts is correlated with the coating's weather resistance. UV radiation is the primary cause of paint aging in outdoor paints. The UV accelerated aging test can replicate the damage that happens outside for months or even years in days or weeks, simulating the UV portion of sunlight's impact on the coating.

The Accelerated aging test uses higher temperatures to artificially accelerate the aging process, simulating real-time aging and shelf life. While real-time aging is necessary for determining a product's or its packaging's expiration date, accelerated aging is an optional necessity for testing.

UV test chambers can be used to validate the performance of coatings by assisting in the selection of new materials and assessing the effect of material compositions on durability. To prevent losses resulting from weather resistance during usage, the required UV accelerated aging test guarantees the coating's long-term weather resistance. Since sunlight's ultraviolet radiation is the primary source of photodegradation and photoaging in photo goods, it is imperative to test novel materials and products for weather resistance before choosing them.

As seen in Fig.12, and listed in Table 3, the coatings take simulated time variation from 2.5 to 3 weeks before aging fracture (coating failure).

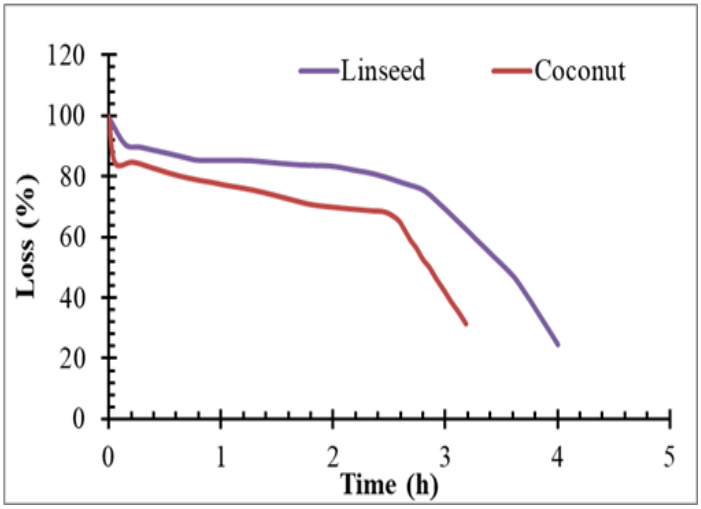

Fig. 12. Aging test for the tested coating

Table 3. Accelerated aging result according to time until coating failure.

Coating	Adhesion (N/mm)	Aging (weeks)
Linseed	0.68	2.85
Coconut	0.64	2.57

3.3.5 Color Change Monitoring

Monitoring the color change of the tested coatings after accelerated aging (accelerating aging) test The color change of the tested coatings on the surface of the tested slides was calculated after exposure to accelerated aging test conditions And recorded in Table 4 and Fig. 13. , according to the (CIE L-a-b) system through the equation [26]: -

$$\Delta E = \sqrt{(\Delta L)^2 + (\Delta a)^2 + (\Delta b)^2}$$

Table 4. Color Change ΔE after 3 weeks of the tested coating (MOC) accelerated aging

Tested coating (MOC)	ΔE after 1 week	ΔE After 2weeks	ΔE after 3 weeks
Blank	*13.52*	*13.68*	*14.21*
Linseed modified coat (MOC)	*2.56*	*4.56*	*4.92*
Coconut modified coat (MOC)	*3.32*	*5.68*	*7.36*

3.3.6 The historical lamp post (case study) before and after applied coating

Based on the previous results of the studied coatings, the best coatings were selected that achieved superior results in terms of corrosion resistance, accelerated aging resistance, and ultraviolet radiation resistance. The modified flaxseed coating (MOC) was the best; hence, it was used in the painting and insulation of the artifact under study (the archaeological lamp post), The following figure Fig. 14: illustrates the historical lamp post before and after the application of the coating (linseed modified coat (MOC) coating)

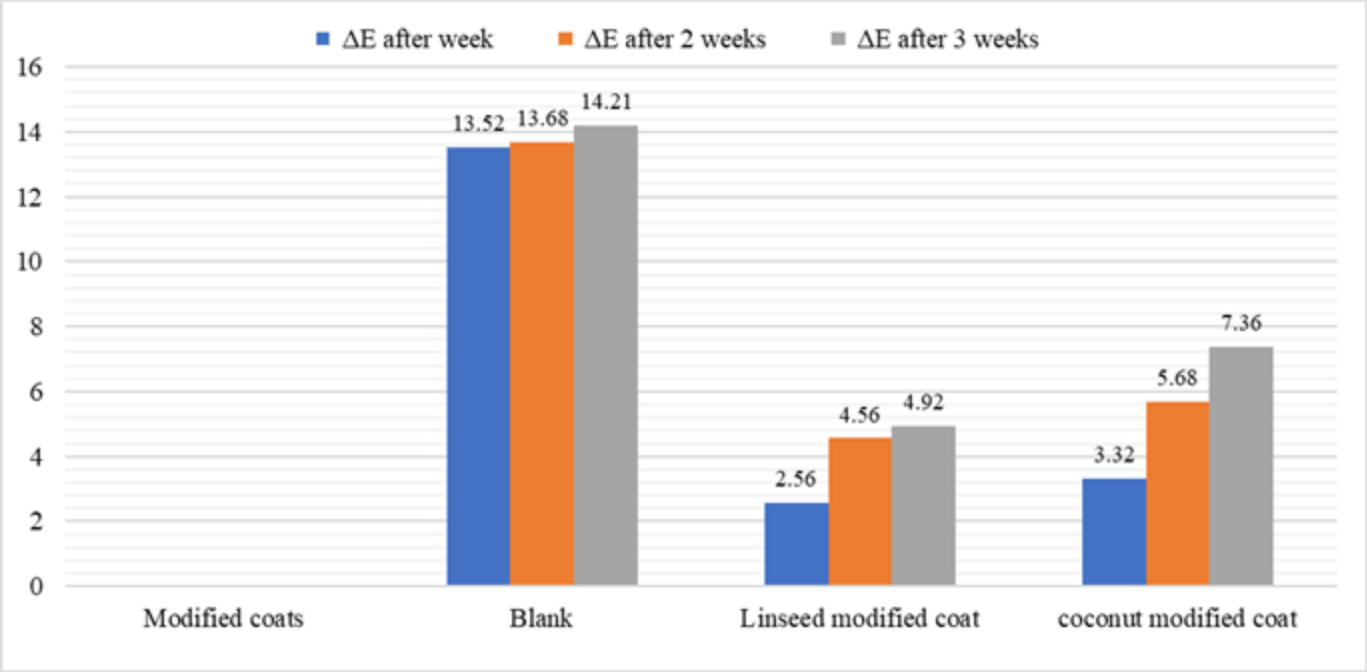

Fig. 13. Color Change ΔE after 3 weeks of the tested Coating (MOC) accelerated aging.

Fig.14. illustration the archaeological lamp post lying in one of the palace's halls (Al-Shennawy Palace) during the restoration works. 'A' represents the lamp post during the restoration process and before the application of the coat, while 'B' shows the column after the completion of the restoration works and the application of the coat as a final protective layer."

Conclusion

In the present study, VO derivatives (*TGO, and MOC*) of linseed, and coconut oil was laboratory synthesized via condensation reaction and chemically confirmed using various spectroscopic techniques such as IR and UV. Using various EMs, the produced TGO and MOC coating for LCS in a 3.5% NaCl solution was assessed. This evaluation demonstrated the effectiveness of both materials in mitigating LCS damage and their protective role. According to PDP measurements, organic coatings prevent corrosion by creating a barrier between the metal and its surroundings, but TGO and MOC delay LCS corrosion by obstructing the anodic and cathodic sites. This suggests mixed protection. This barrier prevents the metal from reacting with corrosive agents such as air and humidity [27].

References

1. Artesani A, Di Turo F, Zucchelli M, Traviglia A. Recent Advances in Protective Coatings for Cultural Heritage–An Overview. Coatings. 2020; 10(3):217. https://doi.org/10.3390/coatings10030217

2. MacLeod, I.D. (2014). Metals: Preservation and Conservation. In: Smith, C. (eds) Encyclopedia of Global Archaeology. Springer, New York, NY.

3. Islam, Muhammad & Beg, H. & Jamari, Saidatul. (2014). Development of Vegetable Oil Based Polymers. Journal of Applied Polymer Science. 10.1002/app.40787.

4. Ling, Z., & Zhou, Q. (2023). Synthesis and properties of linseed oil-based waterborne non-isocyanate polyurethane coating. Green Chemistry, 25(23), 10082-10090. The Royal Society of Chemistry

5. Marsi, N., Rus, A.Z., Mohd Razali, I., Samsuddin, S.A., & Abdul Rashid, A.H. (2017). The Synthesis and Surface Properties of Newly Eco-Resin Based Coconut Oil for Superhydrophobic Coating. Solid State Phenomena, 266, 59 - 63.

6. Karak, Niranjan. Vegetable Oil-Based Polymers: Properties, Processing and Applications. Elsevier Science, 20121.Drabiska, N. & Flynn, C. Extraction and separation of unsaturated fatty acids from sunflower oil Extraction and separation of unsaturated fatty acids from sunflower oil. IOP Conf. Ser. Earth Environ. Sci. 680 680, 12063 (2021).

7. De Almeida, N. R., Beatriz, A., de Arruda, E. J., de Lima, D. P., Silva de Oliveira, L. C., & Micheletti, A. C. (2016). Ozonized vegetable oils: Production, chemical characterization and therapeutic potential. In A. Méndez-Vilas (Ed.), The battle against microbial pathogens: Basic science, technological advances and educational programs (pp. 81-91

8. Sadowska, J., Johansson, B., Johannessen, E., Friman, R., Broniarz-Press, L., & Rosenholm, J. B. (2008). Characterization of ozonated vegetable oils by spectroscopic and chromatographic methods. Chemistry and physics of lipids, 151(2), 85–91.

9. Q. H. Zhang, Y. Y. Li, Y. Lei, X. Wang, H. F. Liu, and G. A. Zhang, “Comparison of the synergistic inhibition mechanism of two eco-friendly amino acids combined corrosion inhibitors for carbon steel pipelines in oil and gas production,” Appl. Surf. Sci., vol. 583, no. October 2021, 2022, doi: 10.1016/j.apsusc.2022.152559.

10. - Frias, C. F., Serra, A. C., Ramalho, A., Coelho, J. F. J. & Fonseca, A. C. Preparation of fully biobased epoxy resins from soybean oil-based amine hardeners. Ind. Crop. Prod. 109, 434–444 (2017)

11. Carroll, G.T.؛ Turro, N.J.؛ Koberstein, J.T. (2010). "Patterning dewetting in thin polymer films by spatially directed photo crosslinking". Journal of Colloid and Interface Science. 556–560.

12. ASTM D 4541., Standard Test Method for Pull-Off Strength of Coatings Using Portable Adhesion Testers, Journal of ASTM International, Annual Book of ASTM Standards, Vol. 3, P.46

13. ASTM., Standard D3359-17, Standard Test Methods for Rating Adhesion by Tape Test, Journal of ASTM International, Annual Book of ASTM Standards, 2017

14. ASTM., Standard B117 -11, Standard Practice for Operating Salt Spray (Fog) Apparatus, Journal of ASTM International, Annual Book of ASTM Standards, 2011

15. ASTM., G154-16., Standard Practice for Operating Fluorescent Ultraviolet (UV) Lamp Apparatus for Exposure of Nonmetallic Materials, Journal of ASTM International, Annual Book of ASTM Standards, Vol. 3, P.46

16. Yan, Q., et al. (2021)2. Effect of temperature on corrosion behavior of E690 steel in 3.5 wt.% NaCl solution1. Materials Research Express, 8, 016528

17. Zehra, S., Aslam, R., & Mobin, M. (2022). Electrochemical Impedance Spectroscopy: A Useful Tool for monitoring the Performance of Corrosion Inhibitors. In I. ulhaq Toor (Ed.), Recent Developments in Analytical Techniques for Corrosion Research (pp. 91117). Springer International Publishing

18. Bolton, W. (2004). 12 - Nyquist diagrams. In W. Bolton (Ed.), Instrumentation and Control Systems (pp. 282-289). Newnes.

19. Roskilly, T., & Mikalsen, R. (2015). Chapter Six - Frequency Domain Analysis. In T. Roskilly & R. Mikalsen (Eds.), Marine Systems Identification, Modeling and Control (pp. 123-147). Butterworth-Heinemann.

20. Cui, G., Bi, Z., Wang, S., Liu, J., Xing, X., Li, Z., & Wang, B. (2020). A comprehensive review on smart anti-corrosive coatings. Progress in Organic Coatings, 148, 105821.

21. 21. Montemor, M.F. (2014). Functional and smart coatings for corrosion protection: A review of recent advances. Surface and Coatings Technology, 258, 17-37. https://doi.org/10.1016/j.surfcoat.2014.06.031

22. 22. Li, D., Lin, C., Batchelor-McAuley, C., Chen, L., & Compton, R. G. (2018). Tafel analysis in practice. Journal of Electroanalytical Chemistry, 826, 117-124.

23. 23. Thakur, A., & Kumar, A. (2021). Sustainable Inhibitors for Corrosion Mitigation in Aggressive Corrosive Media: A Comprehensive Study. Journal of Bio-Tribocorrosion, 7, 67. ernon-Parry, K. D. (2000). Scanning electron microscopy: an introduction. III-Vs Review, 13(4), 40-44.

24. 24. Lazorenko, G., Kasprzhitskii, A., & Nazdracheva, T. (2021). Anti-corrosion coatings for protection of steel railway structures exposed to atmospheric environments: A review. Construction and Building Materials, 288, 123115.

25. 25. Buckley, R.R., Giorgianni, E.J. (2016). CIELAB for Color Image Encoding (CIELAB, 8Bit; Domain and Range, Uses). In: Luo, M.R. (eds), Encyclopedia of Color Science and Technology. Springer, New York, NY

26. 26. Alam, M., Akram, D., Sharmin, E., Zafar, F., & Ahmad, S. (2014). Vegetable oil based eco-friendly coating materials: A review article. Arabian Journal of Chemistry, 7(4), 469479. https://doi.org/10.1016/j.arabjc.2013.12.023